Microporous and Mesoporous Materials 317 (2021) 110980

Contents lists available at ScienceDirect

Microporous and Mesoporous Materials

journal homepage: http://www.elsevier.com/locate/micromeso

Unveiling unique structural features of the YNU-5 aluminosilicate family

Yaping Zhang [a], Yi Zhou [a], Tu Sun [a], Pengyu Chen [b], Chengmin Li [a], Yoshihiro Kubota [c], Satoshi Inagaki [c], Catherine Dejoie [d], Alvaro Mayoral [a,e,f,*], Osamu Terasaki [a]

[a] Center for High-Resolution Electron Microscopy (ChEM), School of Physical Science and Technology, ShanghaiTech University, 393 Middle Huaxia Road, Pudong Shanghai, 201210, China
[b] Zhiyuan College & School of Chemistry and Chemical Engineering, Shanghai Jiao Tong University, 800 Dongchuan Road Shanghai, 200240, China
[c] Division of Materials Science and Chemical Engineering, Yokohama National University, 79-5 Tokiwadai, Hodogaya-ku, Yokohama 240-8501, Japan
[d] ESRF – European Synchrotron Radiation Facility, CS40220, Grenoble, 38043, France
[e] Instituto de Nanociencia y Materiales de Aragon (INMA), Spanish National Research Council (CSIC), University of Zaragoza, 12, Calle de Pedro Cerbuna, Zaragoza 50009, Spain
[f] Laboratorio de Microsocopias Avanzadas (LMA), University of Zaragoza, Mariano Esquillor, S/N, Zaragoza 50018, Spain

ARTICLE INFO

Keywords:
Zeolites
Electron diffraction tomography (EDT)
Structure analysis
Rietveld refinement
Spherical aberration-corrected STEM

ABSTRACT

YNU-5 (**YFI** type) is the first zeolite reported with interconnected 12-, 12-, and 8-ring pores showing a remarkable catalytic potential towards the dimethyl ether (DME)-to-olefin reaction. In this work, the structures of the as-synthesized, calcined and dealuminated YNU-5 zeolites, were investigated by various techniques with special emphasis on advanced electron microscopy methods. The frameworks of the three materials were solely determined by three-dimension electron diffraction tomography, and the space group for the three of them was determined to be *Cmmm*, which is of higher symmetry than the previous reported result. Rietveld refinement was performed against synchrotron Powder X-ray diffraction data in order to obtain precise information of the framework and to locate the organic species, cations and water. Additionally, spherical aberration-corrected scanning transmission electron microscopy was employed to study the local fine structure and to indicate surface reconstruction associated to the displacement of the vacancies through the dealumination process. Finally, a minor phase, whose structure was solved by electron microscopy was found to be **MSE** framework type, appeared in all the three YNU-5 materials.

Overall, the electron microscopy analyses reported in the present work provide additional information regarding the YNU-5 structure in terms of space group determination, additional surface terminations and the identification of a minor phase.

1. 1Introduction

Due to the versatile pore size distribution, adjustable particle size and morphology, thermal stability and large specific surface areas, zeolite field is vital and prosperous in both industry and academia. To date, 253 uniqueframework type have been approved by the International Zeolite Association (IZA). YNU-5 (**YFI** type) is the first zeolite with an interconnected 12–, 12–, 8–ring pore system which has a large and continuous space favorable for mass transfer [1]. The structure of YNU-5 was firstly solved based on powder X-ray diffraction (PXRD) assuming the *C*2/*m* (monoclinic, No.12) space group [1].

YNU-5 has been synthesized using **FAU**-type zeolite as part of the starting silica source [1,2] and dimethyldipropylammonium ($Me_2Pr_2N^+$) as organic structure-directing agent (OSDA). Under these conditions, YNU-5 with very high purity can be obtained in a very narrow synthesis window with **MSE**, **MFI** and ***BEA** as its competing phases.

Among the different structural properties of zeolites, the Si/Al ratio is crucial due to its direct relationship on chemical properties such as ion-exchange, hydrophilicity, stability and acidity. Zeolites obtained by direct synthesis usually have high aluminum content. However, the inherent thermal/hydrothermal stability is a common problem for high Al concentration frameworks; in general, high Si/Al ratio (low Al content) frameworks tend to be used as catalysts, while low Si/Al

* Corresponding author. Center for High-Resolution Electron Microscopy (*ChEM*), School of Physical Science and Technology, ShanghaiTech University, 393 Middle Huaxia Road, Pudong, Shanghai, 201210, China.
E-mail address: amayoral@unizar.es (A. Mayoral).

https://doi.org/10.1016/j.micromeso.2021.110980
Received 3 January 2021; Received in revised form 5 February 2021; Accepted 12 February 2021
Available online 18 February 2021

frameworks are mainly used as ion-exchangers. To modify the aluminum content, various post-synthetic dealumination procedures have been developed that increase the Si/Al ratio such as (i) mineral acid treatment [3,4], (ii) steaming method [5–8] or (iii) reaction with the dealumination agent and supplement Si, such as ammonium hexafluorosilicate ($(NH_4)_2[SiF_6]$) [9,10]. For the particular case of YNU-5, the Si/Al ratio of the framework can be increased from 9 to 350 by a simple treatment with nitric acid with different concentrations under reflux while preserving the crystallinity and thermal stability [2]. Because of the unique structural parameters, excellent thermal stability and tunable Si/Al ratio, YNU-5 displays outstanding performance for the conversion of dimethyl ether to propylene, butylene or other light olefins [1]. In fact, YNU-5 is a suitable material for solid acid catalysis due to its controllable Si/Al ratio, which was found to strongly influence the conversion of dimethyl ether obtaining high values at a short time of stream (TOS), 5 min, that rapidly decreased as the TOS was increased. However, this aspect could be improved by modifying the Si/Al ratio and by introducing a small amount of an impurity phase [1,11].

In order to further developing the catalytic properties of zeolites, a deep structural understanding down to the atomic level is required. In this sense, electron microscopy shows special advantages in structural characterization at the nanoscale such as: (i) diffraction and image information can be obtained simultaneously; (ii) coulomb interaction is much stronger with matter than X-ray's scattering. Therefore, to achieve the same intensity, X-Ray needs around 10^8 times more sample amount in volume in comparison with electron microscopy [12]; (iii) electrons are matter waves with much shorter wave length, therefore high spatial resolution can be achieved.

Furthermore, with the implementation of continuous automated rotating sample holders, it is possible to achieve three-dimensional electron diffraction tomography from small crystals that can be assumed as single crystal particles. Subsequently, combining these data with direct methods, several zeolite frameworks [13–20] have been solved without the necessity of obtaining large single crystals. In addition, imaging in high-resolution mode can provide unique local information of the framework, structural defects or of surface terminations [21–26].

In the present work, we have investigated YNU-5 by advanced electron microscopy methods solving the structure of the three materials (as-synthesized, calcined and dealuminated) by three-dimension electron diffraction tomography (3D-EDT) to evaluate the possible differences among them and to compare with the previous reported data. Rietveld refinement against powder X-ray diffraction data allowed further analysis of the OSDA location, the extra-framework cations and the water content. The local structure was studied by C_s-corrected STEM at atomic level, which allow the identification of substantial differences on the crystal surfaces before and after the dealumination process.

Finally, an additional minor phase was detected both on scanning electron microscopy (SEM) and on transmission electron microscopy (TEM). Its structure was solved by 3D-EDT as **MSE** framework type.

2. Experimental section

2.1. Sample preparation

YNU-5 materials were prepared according to the reported procedures [1,2]. YNU-5 zeolite was synthesized using **FAU** type zeolite as Si and Al sources, $Me_2Pr_2N^+OH^-$ as the OSDA and aqueous solutions of NaOH and KOH as alkaline additives. Colloidal silica was also added to adjust the input Si/Al ratio. The resulting mixture was placed in a Teflon-lined autoclave and heated statically in a convection oven for 165 h at 433 K. The resulting material was collected by filtration, extensively washed with deionized water and dried overnight. The calcined YNU-5 was obtained by heating the as-synthesized YNU-5 in a muffle furnace at 823 K for 6 h after raising the temperature from room temperature to 823 K with a ramp rate of 1.5 K min^{-1}. The De-Al YNU-5 was obtained by

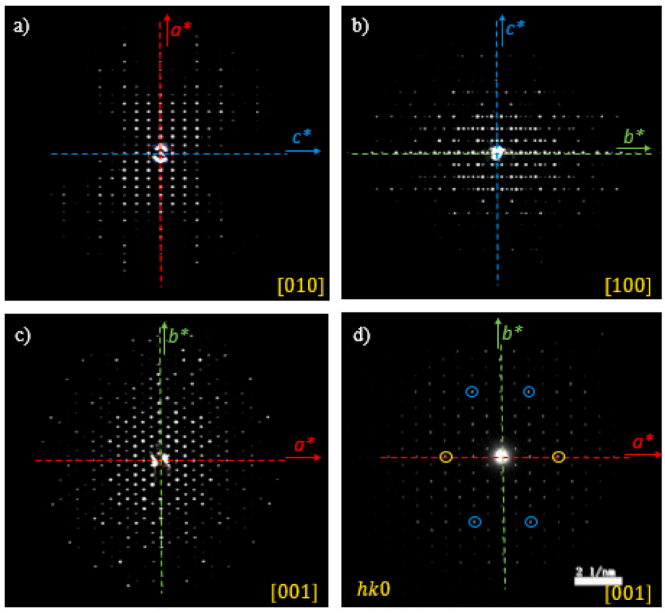

Fig. 1. Electron diffraction patterns of as-synthesized YNU-5. Projected diffraction patterns obtained from 3D-EDT along a) [010]; b) [100] and c) [001] directions. d) Selected area electron diffraction (SAED) pattern along [001] direction. The dashed lines are mirror planes and the circles in figure d) with the same colors mark the strong spots that should have the same intensity according to the Laue class for orthorhombic system. (For interpretation of the references to color in this figure legend, the reader is referred to the Web version of this article.)

treatment with a 13.4 mol L^{-1} HNO_3 solution at 403 K in an oil bath for 24 h.

2.2. Electron microscopy observations

Electron microscopy. For electron microscopy analyses, the samples were firstly crushed for 15 min using agate mortar and pestle, with the intention of obtaining very thin crystals, dispersed in HPLC ethanol by ultrasonic treatment and then few drops of the suspension were placed onto a carbon-coated copper grid. SAED patterns, high-resolution transmission electron Microscopy (HRTEM) images and 3D-EDT data were collected in JEM-2100 Plus in TEM mode at 200 kV with a TVIPS F416 camera using the JEOL.Shell software by Analitex.

For the 3D-EDT experiments, the data sets were collected using a high-angle titlt holder. A nanocrystal was tilted along one axis at a constant speed from $-60°$ to $60°$ within 8 min for each set of data. The reciprocal spaces were reconstructed and the unit cell parameters and diffraction intensities were extracted afterwards.

The SEM images were collected on JSM 7800F Prime with a work distance of 7 mm and landing voltage of 1.00 kV.

C_s-corrected STEM high-angle annular dark field (HAADF) images were taken in a JEOL JEM-ARM300F operated at 300 kV equipped with a cold field emission gun (FEG), and double C_s correctors for TEM and STEM measurements.

2.3. Sample characterization

Si, Al, K analysis. The chemical composition corresponding to Si, Al, K was measured by inductively coupled plasma atomic emission spectrometry (ICP-AES; Thermo Fisher iCAP 7400). 5.040 mg/5.035 mg/5.043 mg of as-synthesized YNU-5/calcined YNU-5/De-Al YNU-5 were dissolved in 2 mL HCl (conc.) and 0.5 mL HF (40%) aqueous solution, respectively. Then, the samples were diluted in water in three 50 mL volumetric flasks. Three different characteristic spectrum peaks were

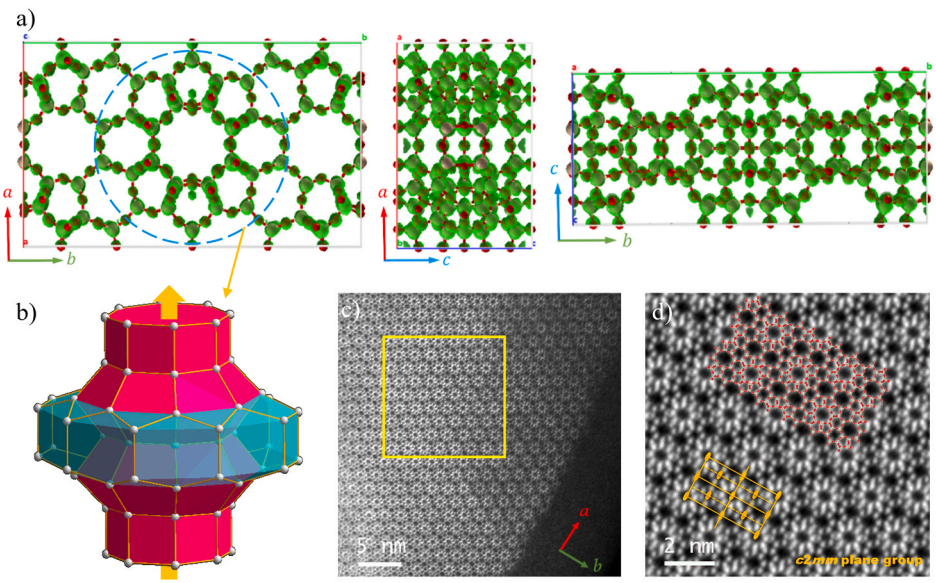

Fig. 2. a) Complete framework solved from as-synthesized YNU-5 3D-EDT data set. Color scale: red, oxygen; yellow, "T" (Si/Al). The green surface covered outside the atom is the electrostatic potential map reconstructed from 3D-EDT data. b) Structure model of the area within blue circle in a). c) Cs-corrected STEM-ADF image of YNU-5 as-synthesized; d) Averaged high-resolution image with *p*1 symmetry of the yellow region in c). The plane group *c*2*mm* is marked with yellow color. (For interpretation of the references to color in this figure legend, the reader is referred to the Web version of this article.)

chosen for each element for element type determination.

C, H, N analysis. C, H, N composition was analyzed using a PerkinElmer 2400 (Clarus 580) operated at 975°*C*. Each sample was tested at least twice in parallel to ensure repeatability.

PXRD collection. High-resolution powder diffraction data of YNU-5 samples were collected at the ID22 beamline at the European Synchrotron Radiation Facility (ESRF) using a wavelength of 0.40003952 Å. Rietveld structure refinement and Pawley refinement were carried out using the *Topas6* software [27].

FT-IR collection. Fourier Transform Infrared Spectroscopy was used to study the structure YNU-5 materials in order to identify different molecules. These measurements were performed using a PerkinElmer Frontier spectrometer in the range of 400–4000 cm^{-1} with a step width of 1 cm^{-1} and 16 scanning times for each step and each sample.

3. Results and discussion

3.1. Framework determination

3D-EDT enables to collect single crystal diffraction analysis from a nanocrystal. Therefore, a Bravais lattice witht he unit cell parameters and Laue-class can be obtained not only from the distribution of the diffraction spots, but also from the distribution of their intensity.

For the as-synthesized YNU-5, Fig. 1a–c corresponds to the electron diffraction (ED) patterns extracted from the 3D-EDT along the [010], [100] and [001] projections respectively, where mirror planes are marked by dashed lines. Even though from diffraction distribution, the lattice type may be trigonal, hexagonal or orthorhombic, in the reconstructed reciprocal space processed by 3D-EDT data, the symmetry of the intensity distribution along [001] indicates a *C*-centered orthorhombic Bravais lattice with unit cell parameters; $a = 18.67$ Å, $b = 32.37$ Å, $c = 12.80$ Å, and $V = 7736$ $Å^3$ that after refinement against PXRD turned to be $a = 18.12514$ (4) Å, $b = 31.75158(7)$ Å, $c = 12.62636(3)$ Å, and $V = 7266.49(3)$ $Å^3$ (Table S1) and *mmm* Laue class, where the mirror planes are marked by dashed lines (Fig. 1c and d).

Among the possible space groups, *Cmmm*, *Cm*2 *m*, *Cmm*2, *C*222, the highest symmetry, *Cmmm*, was selected using standard direct method in *Sir2014* software [28]. Fig. 2a displays the model, along the main crystallographic zone axes *c, b and a*, based on the obtained structural solution, with oxygen atoms in red and "T" atoms in yellow wrapped in green electrostatic potential map. The characteristic 8-ring channel can be observed along the *c* axis (indicated by a blue dashed circle in Fig. 2a and by a yellow arrow in Fig. 2b). The model in Fig. 2b corresponds to the single straight 8-ring channel. Six 5-rings (5^6Rs) and two 6-rings (6^2Rs), colored in pink in Fig. 2b surround the straight 8ring channel, in light transparent blue color. Calcined YNU-5 and De-Al YNU-5 frameworks were also successfully solved assuming the same space group *Cmmm* (see Table S1).

Spherical aberration corrected scanning transmission electron microscopy (C_s-corrected STEM) coupled with an annular dark field detector (ADF) was employed to analyze the crystal framework of the as-synthesized YNU-5. Fig. 2c depicts the atomic observation along the [001] orientation, from which the *c*2*mm* can be directly inferred, Fig. 2d, confirming that the *Cmmm* space group should be adopted, where the ellipse represents the 2-fold rotation axis normal to the paper and the solid lines represent mirror plane and the dashed lines represent the axial glide lines (1/2 along line parallel to projection plane) for the *c*2*mm* symbol. The schematic model obtained from the diffraction data has been overlaid corroborating a perfect matching between the data obtained from diffraction with the atomic-resolution image.

A layer of amorphous carbon can be observed in Fig. 2c; it is attributed to a contamination effect that took place over some zeolite crystallites. Despite that the sample preparation conditions were kept as clean as possible, some carbon compounds from the environment could fall over the TEM grids, especially if the samples were not directly transferred to the electron microscopy column after preparation. To be sure that the layer observed in some of the crystallites was present before irradiation and it corresponded to impurities and not due to beam damage, some crystals were imaged directly before exposing them to any electron beam interaction observing that the layer was already present.

3.2. Extraframework species

ICP-AES and organic element analyzer were used to obtain the chemical composition, Table S2. The chemical compositions obtained were: (i) As-synthesized YNU-5: $Si_{109}Al_{11}K_{5.7}C_{45}H_{141}N_6O_{222}$; (ii) Calcined YNU-5: $Si_{108}Al_{12}K_{5.9}$ $C_{5.1}H_{109}O_{275}$; (iii) De-Al YNU-5: $Si_{108}Al_{0.48}C_{16.4}H_{76}O_{239}$. As-synthesized YNU-5 contains 6 OSDA and around 6 K^+ per unit cell. After calcination, the OSDA was removed and the calcined YNU-5 contains around 50 water molecules per unit cell.

After obtaining the framework structure by 3D-EDT, more detailed information of guest molecules or cations was obtained by Rietveld refinement against synchrotron PXRD data using *TOPAS6* [27] with the framework solved from 3D-EDT as the initial model. The presence of extraframework species mainly influences the diffraction intensities of

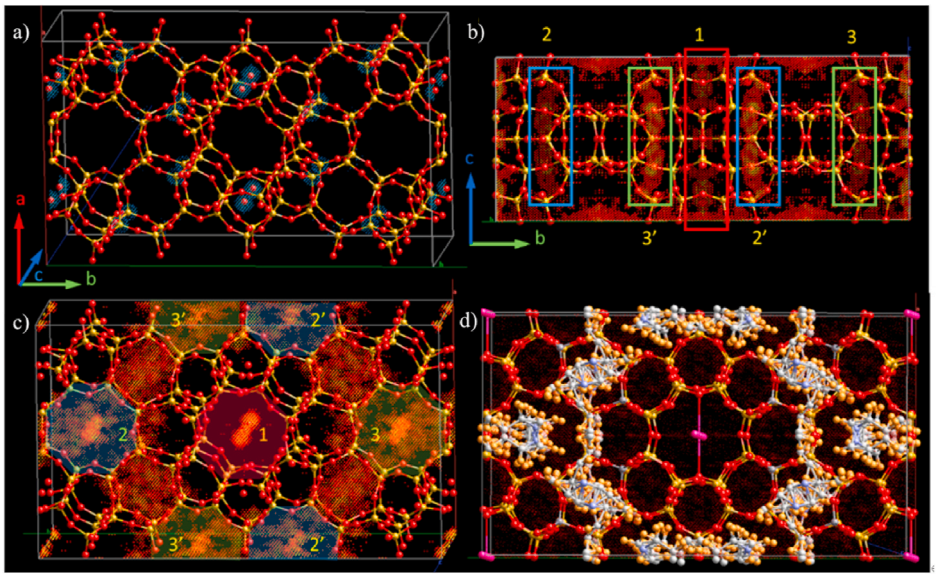

Fig. 3. Rietveld refinement for as-synthesized YNU-5 (red, oxygen atoms; yellow, silicon atoms; pink, potassium atoms). a) Fourier difference map obtained from the PXRD with data range 6–30°; b), c) Fourier difference map obtained from the PXRD with data range 2–30°; d) Final structure model from Rietveld refinement with range 2–30°. (For interpretation of the references to color in this figure legend, the reader is referred to the Web version of this article.)

low angle reflections. During the refinement process, a 2θ range between 6° and 30° was firstly used to refine the framework atomic positions and the scale parameter. Then, the entire structure, including the extra-framework species (OSDA, water molecules, and K atoms), was refined using the complete 2°–30° 2θ range.

3.2.1. *As-synthesized YNU-5*

Assuming that all "T" sites (T = Si, Al) can be either occupied by Si or Al with equal probability, the negative cloud (blue color) and the positive one (orange) observed in the Fourier difference maps, Fig. 3a–c, may correspond to a possible vacancy or Al site for the negative signal and to the presence of the OSDA or K^+ for the positive one.

Thus, the positive cloud can belong either to the K^+ or to the OSDA. In Fig. 3b and Fig. 3c three 8-rings are marked as **1**, **2**, **3** red, blue and green rectangles in Fig. 3b and with translucent colored (same color code) octagons in Fig. 3c. The 8Rs marked **2** and **3** are symmetry related by a mirror plane, while **2′** and **3'** are equivalent to **2** and **3**.

In Fig. 3b, for the 8Rs marked as **2** and **3**, the cloud signals are continuously curving; meanwhile in **1**, the cloud signal is straight and not continuous. Therefore, it is reasonable to assume that K^+ is located in the channels **1**, and, it was introduced in the model. The OSDA was then placed in the other channels (**2** and **3**). The simulated annealing method was used to obtain the location and conformation of the OSDA molecules, and the structure was then refined. 96.3% of the K^+ (5.49 K^+ compared with 5.7 K^+ from chemical element analysis) were located in channel 1. A good match for the OSDA was also retrieved (6 and 6.0 molecules per unit cell obtained from PXRD and chemical analysis, respectively). The final structure is displayed in Fig. 3d, with the K^+ represented as pink spheres and the OSDA in white for H, yellow for C and purple for N.

3.2.2. *Calcined YNU-5*

For the calcined YNU-5, as there was no OSDA, the positive signal obtained was directly attributed to the K^+ cations that were located inside the straight 8Rs denoted as number 1 in Fig. 3b and Fig. 3c. The final Rietveld refinement structure is presented in Fig. S1. For this material, the water content significantly increased up to 11–12 wt% as a consequence of OSDA removal and subsequent hydration from the atmosphere, which was not found in the 8R channel (Fig. 2b yellow arrow) in agreement with the results from NMR analysis reported in the literature [2]. According to the Rietveld refinement, the water molecules filled the empty space left by the OSDA molecules. The amount of water ($53H_2O$ molecules per unit cell) and K^+ (5.77 K^+ compared with 5.9 K^+ from chemical element analysis) matched well with the chemical element analysis data.

3.2.3. *De-Al YNU-5*

For De-Al YNU-5, most of Al atoms were removed (Si/Al ratio = 305) and no K^+ was detected. A Pawley refinement (Fig. S4) was performed to determine the unit cell parameters, Table S1. For each Al removed from the framework, there will be a silanol nest left around that vacancy if there are no other atoms to supplement that position.

FT-IR analyses of the three samples are presented in Fig. S2. By checking the range between 1350 and 4000 cm^{-1}, significant differences were evidenced. For as-synthesized YNU-5 (Fig. S2a), a strong and sharp band appears at 1500 cm^{-1} corresponding to the positively coordinated N that belong to the OSDA. This band almost completely disappeared after calcination, Fig. S2c. However, another band appeared at the same wavenumber for the De-Al YNU-5 (Fig. S2e) associated to some NO_3^- molecules that remained after the dealumination process with nitric acid.

At higher energies, the vibrations corresponding to the [SiO–H] and [SiO–H···OH] groups appeared around or above 3650 cm^{-1} [29]. For as-synthesized YNU-5, a very weak band was observed at around 3650 cm^{-1} which significantly increased and widened for calcined YNU-5 (Fig- S2c) due to the aggregation of [O–H] through hydrogen bonding ([SiO–H···OH] groups). Finally, very sharp bands appeared in the De-Al YNU-5 spectrum (Fig. S2e) associated to the formation of [SiO–H] groups.

On the other hand, in the region between 400 and 1350 cm^{-1}, the most significant difference was observed around 950 cm^{-1} which is associated to the existence of Si–OH vibrations [30]. No band was detected for the as-synthesized YNU-5 and calcined YNU-5 (Figs. S2b-d), suggesting the absence or very low content of silanol groups. However, because of the dealumination process [Si–OH] were generated in De-Al YNU-5, and correspond to the signal at around 950 cm^{-1} (Fig. S2f). [Si–OH] and [SiO–H] bands due to the dealumination procedure are marked with red character in Figs. S2e and S2f [31,32].

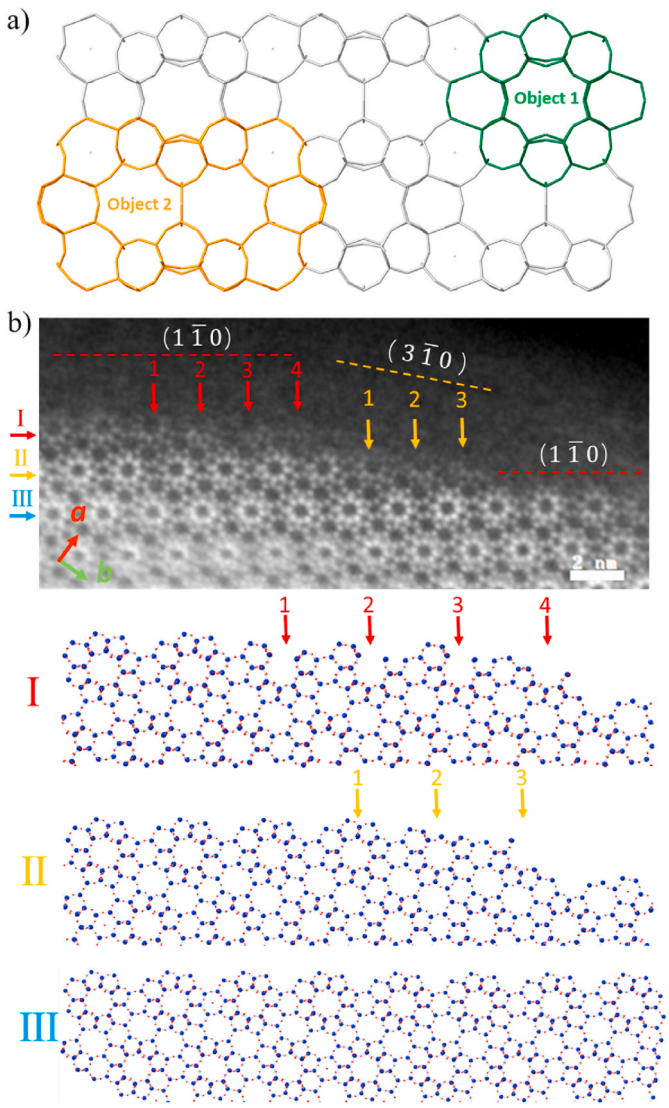

Fig. 4. Termination structure of as-synthesized YNU-5 crystal. a) Schematic drawing of the as-synthesized YNU-5 framework along [001], with two proposed building units (objects **1** and **2**) marked in different colors, green and yellow, respectively. b) Cs-corrected STEM-ADF image of the termination of a YNU-5 crystallite. Crystal termination models of different layers (layer **I**, **II**, **III**) is displayed below the STEM-ADF image. (For interpretation of the references to color in this figure legend, the reader is referred to the Web version of this article.)

3.3. Surface fine structures

Besides the excellent spatial resolution that (Scanning) Transmission electron microscopy provides [22,25], this methodology also allows the characterization of the surface termination of the crystals, unraveling unique details (for the shake of clarity; hereafter, the all "T" atoms in the models will be colored in blue instead of yellow as it was done in the structure analysis part). For YNU-5, Nakazawa and co-workers [1] proposed certain surface terminations of the calcined YNU-5, the surface was perfectly flat formed by complete units denoted in that work as *object **1***, colored in green (composed of 8Rs surrounded by 5 and 6Rs when observed along the [001] projection) see Fig. 4a, green unit. Additionally, they also proposed that the outermost surface could also terminates with these fully formed *objects **1*** and in between incomplete units of the so-called *object **2*** (Fig. 4a, orange color). In here, we have analyzed the different surface terminations along the distinct facets for the as-synthesized and for De-Al YNU-5 along the [001] projection and

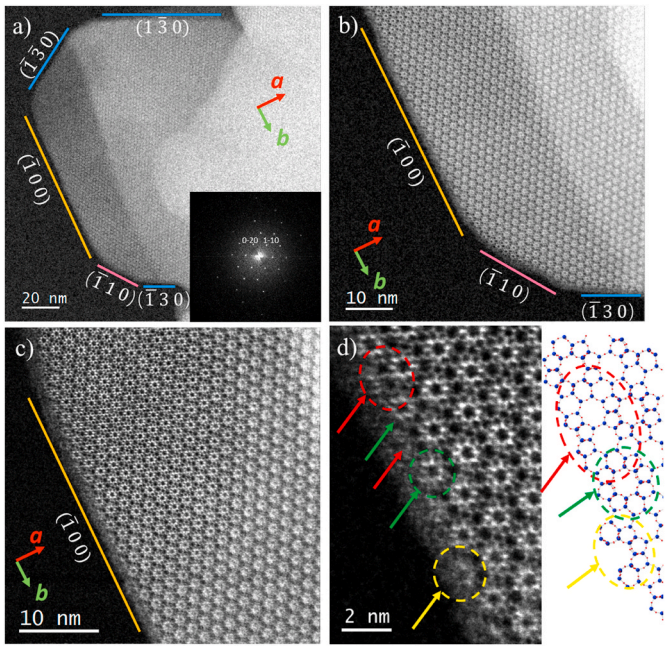

Fig. 5. C_s-corrected STEM-ADF data of as synthesized YNU-5 along the [001] zone axis. a) Low magnification image with the Fourier diffractogram (FD) inset. b) Edge of the crystal showing the ($\bar{1}$00), ($\bar{1}$10) and ($\bar{1}$30) facets. c) Zoomed in view of the ($\bar{1}$00) facet. d) Analysis of the crystal surface at atomic level, with different types of termination marked by colored arrows. The model with similar structure is also presented using the same color coded arrows to point out different terminations. (For interpretation of the references to color in this figure legend, the reader is referred to the Web version of this article.)

compared the results among themselves and with the previous reported data completing the series of YNU-5.

3.3.1. As-synthesized YNU-5 surface analysis

Fig. 4b displays the C_s-corrected STEM-ADF (along [001] zone axis) image of the (1$\bar{1}$0), (3$\bar{1}$0) facets, where the existence of surface steps from different layers denoted as **I**, **II** and **III** are evidenced. These steps correspond to what it can be deduced as a building unit for YNU-5, which would correspond the *object **1***, in agreement with the data reported by Nakazawa et al. However, in here, such unit was observed at different growing steps (resulting in different termination sites) pointed by numbered arrows, Fig. 4b. For the outermost layer named as **I**, the arrow numbered as **1** shows the first non-complete *object **1***, where two of the top 5Rs were not formed; in this case, the surface termination corresponded to a 6R and a 5R with the 8Rs opened. The next unit denoted here with number **2**, exhibits a very similar termination with opened 8Rs and where the 5Rs which were fully formed are now also incomplete leading into a more opened termination. The next unit, number **3**, is the same as number **2** with the 8Rs and the 5Rs not completed. Finally, number **4** corresponds to the last unit observed in this step; in this case, it can be appreciated a barely formed *object **1***, with only 5^3Rs fully formed. This observation was slightly different than the one reported by Nakazawa, where they only visualized complete *object **1*** units for the same {110} facets.

The following step denoted here as **II** is also composed by both complete and not fully formed *objects **1*** units. In this layer, number **1** has been marked as a fully formed *object **1*** unit. Number **2** corresponds to a termination where the 8R is fully formed but not the units which compose it; thus, the two 5Rs on top are not complete. The last unit of this step displays an open 8R with three of the 5Rs missing and one of the 6R opened due to its incompleteness.

Finally, the last step, **III**, is fully formed by complete *objects **1*** in a similar termination as that one described by Nakazawa [1].

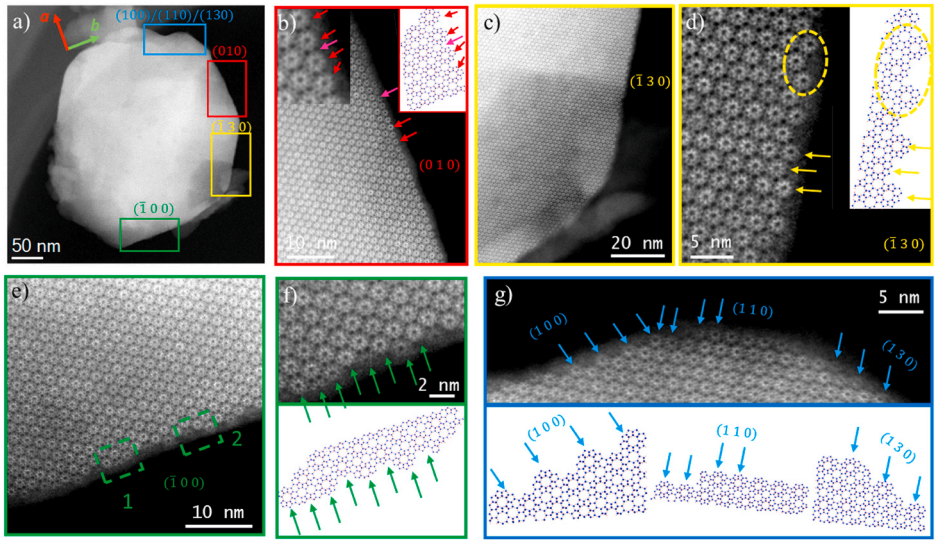

Fig. 6. C_s-corrected STEM-ADF observation of dealuminated YNU-5. a) Low magnification image with the areas analyzed marked by colored rectangles. b) Closer observation of the (010) facet with a magnified image and the schematic model shown inset. c) and d) High-magnification images of the ($\bar{1}$30) termination. The yellow arrows point at the different termination units. The schematic surface termination is shown inset in d). e) and f) Close-up observation of the ($\bar{1}$00) surface. g) Magnified region of the top part of the crystal with different facets identified (100), (110) and (130). The blue arrows indicate the different termination units in the experimental data and in the different models for each surface. (For interpretation of the references to color in this figure legend, the reader is referred to the Web version of this article.)

Fig. 5 depicts an entire YNU-5 particle of around 140 nm sitting on its [001] zone axis, the different surface facets are marked with ($\bar{1}$00), ($\bar{1}$10), (1$\bar{3}$0) and ($\bar{1}$30), Fig. 5a and Fig. 5b correspond to a closer observation of these facets, for the ($\bar{1}$10), a surface step similar to the observation presented in Fig. 4 can be visualized. In addition, a magnified observation of the ($\bar{1}$00) facets is depicted in Fig. 5c, observing a nearly flat surface. In order to have such an almost flat surface, the space between the *object* ***1*** units should be filled by *objects* ***2*** as described by Nakazawa [1]. In our work; however, the *objects* ***2***, which are intercalated between *objects* ***1*** are fully formed, as denoted by red arrows in Fig. 5d. Furthermore, partially formed *objects* ***1*** can be also identified, confirming that the surface termination on the {100} and on the {130} facets are formed by fully formed *objects* ***2***, partially formed *objects* ***1*** (yellow arrows) and fully formed *objects* ***1*** (green arrows). For a better understanding a schematic representation of the structure is presented with the termination units also indicated by dashed circles. This observation suggests that the growth formation of YNU-5 takes place through a two dimensional assembly, where layers of complete *objects* ***2*** and *objects* ***1*** form a nearly flat surface, on which the next layer would start to grow (as partially formed units) on a new plane of the layered structure.

3.3.2. De-Al YNU-5 surface analysis

It has been reported the excellent crystallinity and thermal stability of the De-Al YNU-5, which can be achieved after acidic treatment (nitric acid) at temperatures higher than 100 °C, as a consequence of Si-migration, which would terminate with the Si atoms from the surface of the crystals. However, no evidence of surface reconstruction has been proved yet. In here, we have studied the atomic configuration of the surface for the De-Al YNU-5 in the same way as we did it for the as-synthesized material. Fig. 6a exhibits the low-magnification image of an entire particle sitting on the [001] zone axis with dimensions of around 340 nm × 240 nm. The different facets of the crystal have been denoted by colored rectangles with the correspondent indexing. Flat surfaces are observed for the (010) termination, Fig. 6b, in a similar manner as it was observed for the {110} termination of the as-synthesized YNU-5 (Fig. 4b, surface denoted as **III**), formed by complete *objects* ***1***, marked by red arrows, which were subsequently linked by *object* ***2*** units that were not fully formed, pink arrow. For a clearer visualization of the surface termination, a magnified region together with the model indicating the same units as experimentally observed are shown inset. More interestingly, it is the surface termination observed for the ($\bar{1}$30) facets, Fig. 6c and Fig. 6d; in this case, a *zig-zag* arrangement was present which was not detected for the as-synthesized material. The building units responsible for this formation are marked by a yellow dashed oval and by yellow arrows, Fig. 6d. In this case, the most significant difference with the parental YNU-5 is that the building units that would be in between two *objects* **1** that would correspond to an *object* ***2*** were missing. This is also evidenced in Fig. 6e and f which correspond to the ($\bar{1}$00) facets. Fig. 6e exhibits the region indexed as ($\bar{1}$00) facet, where the two types of terminations can be observed marked with dashed rectangles numbered **1** and **2**.

The amplified micrograph is depicted in Fig. 6f where the different ending units together with its schematic model are pointed by green arrows. The region marked as **1** corresponds to the termination already observed in Fig. 5 along the {100} and {110} surfaces and in the data reported by Nakazawa [1], where a fully formed *object* ***2*** was formed in between two *objects* ***1***. On the other hand, a *zig-zag* surface was also identified for this facet that would correspond to the missing *object* ***2***. This effect was also observed for additional (100) and (130) surfaces observed at the top of the crystal, Fig. 6g. In this region, the morphology was a truncated triangle with a flat (110) termination observed between the (100) and the (130) facets where in both cases the missing *objects* ***2*** were evidenced. The schematic representation of each of the three facets is also displayed pointing, blue arrows, at the *object* ***1*** units.

3.3.3. Surface change after dealumination

As already mentioned, during the dealumination process it would be expected that vacancies would be generated within the framework decreasing the thermal stability. This effect was observed for sample processed at low temperatures (80 °C) [2]. However, for higher temperatures the thermal stability and in consequence the crystallinity was maintained and even improved. From the electron microscopy perspective, the dealuminated material was very similar to the as-synthesized sample displaying very good crystallinity and similar electron beam stability. Such a good thermal stability was explained in terms of Si-migration; for this to occur, Si atoms would be hydrolyzed creating monosilicic species ($Si(OH)_4$) that would enter in the framework in the site defects (aluminum vacancies) via condensation. The new vacancy created would be then filled by another Si that would hydrolyze and condensate in the same manner. After repeating this process several times, the defects would “move” towards the surface, where they could be visualized.

From the observations carried out on the De-Al YNU-5, the defects generated on the surface are primarily associated to the *object* ***2*** units that, based on the experimental evidence, would be more subjected to be hydrolyzed than the *objects* ***1***. In fact, after performing the Rietveld

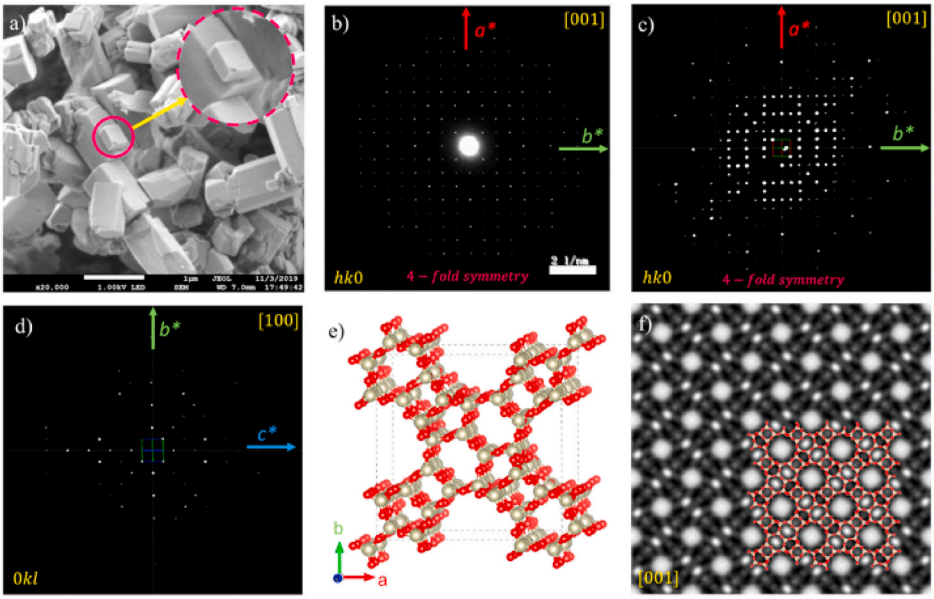

Fig. 7. EM data on minor phase. a) SEM image of as-synthesized YNU-5 sample, in which a small crystal shows tetragonal morphology. b) 4-fold symmetric SAED pattern of minor phase along [001] direction. The extinction condition cannot be easily judged from the pattern due to the serious dynamic scattering effect. Slice view of 3D-EDT data of the tetragonal minor phase c) along [001] and d) along [100]. e) Structure model of minor phase solved from the 3D-EDT. f) *p*4*g* plane group averaged HRTEM image of minor phase along [001] direction.

refinement of the calcined YNU-5 (containing a high amount of water) it was found that the straight 8-rings were more hydrophobic and less subjected to accommodate water molecules. This observation is also in agreement with the ^{27}Al DE MAS NMR spectra analyses carried out for different dealumination conditions, where they suggested that the atoms inside the isolated 8-rings channels (the inner part of the *object* ***1***) were less subjected to be hydrolyzed because the diffusion of water along these channels may be restricted. Although there are still quite a number of vacancies left due to the dealumination process according to the FT-IR spectrum, this mechanism does improve the stability of the De-Al YNU-5.

3.4. Minor phase in YNU-5 samples

Although the H_2O/Si ratio was controlled very carefully during the synthesis process, there was several small peaks in the PXRD pattern that could not be indexed with the refined cell parameters in all the three samples, suggesting the existence of another phase (Fig. S4). Several crystals with tetragonal morphology that differed from the common morphology of YNU-5 were found in the SEM data (Fig. 7a). However, the content of this phase determined by PXRD was less than 0.2 wt% (Fig. S4); therefore, the diffraction intensity could not be used to solve it. For this analysis, TEM is very advantageous over PXRD as it allows the analysis of single crystallites. The SAED pattern along a certain direction exhibited a clear 4-fold symmetry which did not belong to the YNU-5 structure, Fig. 7b. Through 3D-EDT data, the unit cell parameters were determined to be a = b = 18.2 Å, c = 20.7 Å, α = β = γ = 90°, confirming the tetragonal symmetry, (Fig. 7c and d). The reflection conditions could be summarized as: 0 kl: $k + l = 2n$, 00l: $l = 2n$, h00: $h = 2n$, with only three possible space groups that could satisfy these conditions: $P4_2nm$ (No.102), P-4n2 (No.118) and $P4_2/mnm$ (No.136). Since the three of them belong to the same Laue class but different point group, $P4_2/mnm$ with the highest symmetry was adopted for structure solution from the 3D-EDT data. These results were in agreement with the **MSE** topology (Fig. 7e). Furthermore, HRTEM data taken along [001] direction (Fig. 7f), exhibited the characteristic arrangement of large pores (12R) and small pores (6R). For direct comparison the schematic model obtained from the 3D-EDT data has been overlaid.

4. Conclusions

In this work, 3D-EDT technique combined with direct methods were used to solve the framework of the as-synthesized, calcined and De-Al YNU-5 zeolites assuming C*mmm* as the space group. High-resolution C_s-STEM analyses supported the solution obtained from 3D-EDT.

Rietveld refinement of the as-synthesized and of the calcined YNU-5 were used to obtain a more precise structure solution including the accurate location of the OSDA, extra-framework cations and water molecules using the *Cmmm* space group. In the absence of specific or definite guest species in De-Al YNU-5, only Pawley refinement was used to obtain precise unit cell parameters.

Based on atomic-resolution image analyses, different surface terminations were identified for the as-synthesized material and for the dealuminated one. The structural defects observed for the dealuminated material could explain the formation and migration of the vacancies created during the dealumination process.

Additionally, a tetragonal minor phase was identified by SEM and TEM observations. This unknown structure, which was present in less than 0.2 wt% according to the PXRD, was solely solved by 3D-EDT to be **MSE** framework type.

CRediT authorship contribution statement

Yaping Zhang: Investigation, Writing, Formal Analysis. **Yi Zhou:** Investigation, Writing, Formal Analysis. **Tu Sun:** Investigation, Writing, Formal Analysis. **Pengyu Chen:** Investigation. **Chengmin Li:** Investigation. **Yoshihiro Kubota:** Investigation, Formal Analysis. **Satoshi Inagaki:** Investigation. **Catherine Dejoie:** Investigation, Formal Analysis. **Alvaro Mayoral:** Conceptualization, Investigation, Writing-Reviewing and Editing, Supervision, Resources. **Osamu Terasaki:** Term, Conceptualization, Resources, Writing-Reviewing and Editing, Supervision.

Declaration of competing interest

The authors declare that they have no known competing financial interests or personal relationships that could have appeared to influence the work reported in this paper.

Acknowledgements

The authors would like to thank to The Centre for High-resolution Electron Microscopy (*ChEM*), supported by SPST of ShanghaiTech University under contract No. EM02161943; to the National Natural Science

Foundation of China (NFSC-21850410448, NSFC- 21835002). AM also acknowledges the Spanish Ministry of Science under the Ramon y Cajal Program (RYC2018-024561-I) and to the regional government of Aragon (DGA E13_20R). The Element component analysis is supported by Lili Du and Na Yu in ShanghaiTech testing analysis platform. YK is grateful to the Japan Science and Technology Agency (JST) for the CONCERT-Japan (grant number: JPMJSC18C4) program, and to the Japan Society for the Promotion of Science (JSPS) for the Grant-in-Aid for Scientific Research (B), grant number 19H02513. We would like to acknowledge Ms Yuka Yoshida of Yokohama National University for the sample preparation and discussion. We would like to thank Peter Oleynikov in AnaliteX company to give the support about the data collecting software and data processing software and also the instruction for us about the 3D-EDT theory.

Appendix A. Supplementary data

Supplementary data related to this article can be found at https://doi.org/10.1016/j.micromeso.2021.110980.

References

[1] N. Nakazawa, T. Ikeda, N. Hiyoshi, Y. Yoshida, Q. Han, S. Inagaki, Y. Kubota, A microporous aluminosilicate with 12-, 12-, and 8-ring pores and isolated 8-ring channels, J. Am. Chem. Soc. 139 (2017) 7989–7997.
[2] N. Nakazawa, Y. Yoshida, S. Inagaki, Y. Kubota, Synthesis of novel aluminosilicate YNU-5 and enhancement of the framework thermal stability by post-synthesis treatment, Microporous Mesoporous Mater. 280 (2019) 66–74.
[3] H.K. Beyer, Dealumination Techniques for Zeolites, Post-Synthesis Modification, 2002, pp. 203–255.
[4] E. Bourgeat-Lami, F. Fajula, D. Anglerot, T.D. Courieres, Single-step dealumination of zeolite-beta precursors for the preparation of hydrophobic adsorbents, Microporous Mater. 1 (1993) 237–245.
[5] J. Scherzer, The preparation and characterization of aluminum-deficient zeolites, Catalytic Materials: Relationship between Structure and Reactivity1984, pp. 157-200.
[6] T. Masuda, Y. Fujikata, S.R. Mukai, K. Hashimoto, Changes in catalytic activity of MFI-type zeolites caused by dealumination in a steam atmosphere, Appl. Catal. Gen. 172 (1998) 73–83.
[7] G.J. Hutchings, A. Burrows, C. Rhodes, C.J. Kiely, R. McClung, Dealumination of mordenite catalysts using a low concentration of steam, J. Chem. Soc. Faraday. Trans. 93 (1997) 3593–3598.
[8] X.X. Zhang, D.G. Cheng, F.Q. Chen, X.L. Zhan, Dealumination kinetics of composite ZSM-5/mordenite zeolite during steam treatment: an in-situ DRIFTS study, Chin. J. Chem. Eng. 26 (2018) 545–550.
[9] D. Suttipat, T. Yutthalekha, W. Wannapakdee, P. Dugkhuntod, P. Wetchasat, P. Kidkhunthod, C. Wattanakit, Tunable acid-base bifunction of hierarchical aluminum-rich zeolites for the one-pot tandem deacetalization-henry reaction, ChemPlusChem 84 (2019) 1503–1507.
[10] L.D. Borges, J.L. de Macedo, Solid-state dealumination of zeolite Y: structural characterization and acidity analysis by calorimetric measurements, Microporous Mesoporous Mater. 236 (2016) 85–93.
[11] Q. Liu, Y. Yoshida, N. Nakazawa, S. Inagaki, Y. Kubota, The synthesis of YNU-5 zeolite and its application to the catalysis in the dimethyl ether-to-olefin reaction, Materials 13 (2020) 2030.
[12] O. Terasaki, T. Ohsuna, Z. Liu, Y. Sakamoto, A.E. Garcia-Bennett, Structural study of meso-porous materials by electron microscopy, Stud. Surf. Sci. Catal. 148 (2004) 261–288.
[13] W. Hua, H. Chen, Z.B. Yu, X. Zou, J. Lin, J. Sun, A germanosilicate structure with 11x11x12-ring channels solved by electron crystallography, Angew Chem. Int. Ed. Engl. 53 (2014) 5868–5871.
[14] T. Sun, L. Wei, Y.C. Chen, Y.H. Ma, Y.B. Zhang, Atomic-level characterization of dynamics of a 3D covalent organic framework by cryo-electron diffraction tomography, J. Am. Chem. Soc. 141 (2019) 10962–10966.
[15] J. Li, J.L. Sun, Application of X-ray diffraction and electron crystallography for solving complex structure problems, Accounts Chem. Res. 50 (2017) 2737–2745.
[16] A. Mayence, J.R.G. Navarro, Y.H. Ma, O. Terasaki, L. Bergstrom, P. Oleynikov, Phase identification and structure solution by three-dimensional electron diffraction tomography: Gd-phosphate nanorods, Inorg. Chem. 53 (2014) 5067–5072.
[17] Y.F. Yun, X.D. Zou, S. Hovmoller, W. Wan, Three-dimensional electron diffraction as a complementary technique to powder X-ray diffraction for phase identification and structure solution of powders, Iucrj 2 (2015) 267–282.
[18] K. J, H. Hauptman, The phases and magnitudes of the structure factors, Acta Crystallogr. 3 (1950) 181–187.
[19] M. Gemmi, P. Oleynikov, Scanning reciprocal space for solving unknown structures: energy filtered diffraction tomography and rotation diffraction tomography methods, Z. für Kristallogr. - Cryst. Mater. 228 (2013) 51–58.
[20] M. Gemmi, M.G.I. La Placa, A.S. Galanis, E.F. Rauch, S. Nicolopoulos, Fast electron diffraction tomography, J. Appl. Crystallogr. 48 (2015) 718–727.
[21] Q. Zhang, A. Mayoral, J. Li, J. Ruan, V. Alfredsson, Y. Ma, J. Yu, O. Terasaki, Electron microscopy studies of local structural modulations in zeolite crystals, Angew. Chem. Int. Ed. (2020) 19403–19413.
[22] A. Mayoral, Q. Zhang, Y. Zhou, P. Chen, Y. Ma, T. Monji, P. Losch, W. Schmidt, F. Schüth, H. Hirao, J. Yu, O. Terasaki, Direct atomic-level imaging of zeolites: oxygen, sodium in Na-LTA and iron in Fe-MFI, Angew. Chem. Int. Ed. 59 (2020) 19361–19721.
[23] A. Mayoral, P.d. Angel, M. Ramos, Electron microscopy techniques to study structure/function relationships in catalytic materials, in: J. Domínguez-Esquivel, M.R. M (Eds.), Advanced Catalytic Materials: Current Status and Future Progress, 2019, pp. 97–128. Springer, Cham.
[24] J.Y. Li, C.Q. Zhang, J.X. Jiang, J.H. Yu, O. Terasaki, A. Mayoral, Structure solution and defect analysis of an extra-large pore zeolite with UTL topology by electron microscopy, J. Phys. Chem. Lett. 11 (2020) 3350–3356.
[25] C.M. Li, Q. Zhang, A. Mayoral, Ten years of aberration corrected electron microscopy for ordered nanoporous materials, ChemCatChem 12 (2020) 1248–1269.
[26] Q.M. Sun, N. Wang, T.J. Zhang, R. Bai, A. Mayoral, P. Zhang, Q.H. Zhang, O. Terasaki, J.H. Yu, Zeolite-encaged single-atom rhodium catalysts: highly-efficient hydrogen generation and shape-selective tandem hydrogenation of nitroarenes, Angew. Chem. Int. Ed. 58 (2019) 18570–18576.
[27] A.A. Coelho, Indexing of powder diffraction patterns by iterative use of singular value decomposition, J. Appl. Crystallogr. 36 (2003) 86–95.
[28] M.C. Burla, R. Caliandro, B. Carrozzini, G.L. Cascarano, C. Cuocci, C. Giacovazzo, M. Mallamo, A. Mazzone, G. Polidori, Crystal structure determination and refinement via SIR2014, J. Appl. Crystallogr. 48 (2015) 306–309.
[29] M. Maache, A. Janin, J.C. Lavalley, J.F. Joly, E. Benazzi, Acidity of zeolites-beta dealuminated by acid leaching - an ftir study using different probe molecules (pyridine, carbon-monoxide), Zeolites 13 (1993) 419–426.
[30] Y. Lei, X. Chen, H. Song, Z. Hu, B. Cao, Improvement of thermal insulation performance of silica aerogels by Al2O3 powders doping, Ceram. Int. 43 (2017) 10799–10804.
[31] E.M. Flanigen, H. Khatami, H.A. Szymanski, Infrared Structural Studies of Zeolite Frameworks, Molecular Sieve Zeolites-, 1974, pp. 201–229.
[32] O. Cairon, S. Khabtou, E. Balanzat, A. Janin, M. Marzin, A. Chambellan, J. C. Lavalley, T. Chevreau, Determination by Ir spectroscopy of the N(Al-fram) and crystallinity level for amorphous phase containing hy zeolites, Zeolites Related Microporous Mater. State Art 84 (1994) 997–1004.